Quantum Electrodynamics

28

Jonathan R. Sapirstein

Contents

Abstract

Theoretical issues in bound state quantum electrodynamics are discussed with emphasis on a unified derivation of radiative and recoil corrections with the use of Green functions.

Keywords

effective field theory · vacuum polarization · Lamb shift · order perturbation theory · Feynman gauge

28.1 Introduction

Quantum electrodynamics (QED) is now understood to be a component of the Standard Model, the theory which describes the strong, weak, and electromagnetic interactions in the framework of quantum field theory (QFT). It was historically the first QFT, describing the interactions of electrons and photons, consistently incorporating quantum mechanics and relativity. Many of the seminal papers on the subject are collected in [1]. Corrections to the lowest order predications of the theory are proportional to powers of α, the fine structure constant. However, difficulties are encountered with ultraviolet divergent integrals when setting up perturbation theory in this small ($\approx 1/137$) parameter, and while the first papers on QED date from 1928, the difficulties were not overcome until 1947 [2]. Once the modern renormalized form of QED was established, work on the perturbation expansion in α could proceed, and efforts by many researchers that continue to the present day have led to theoretical predictions of unparalleled accuracy for a number of systems. The hydrogen atom in particular plays a central role in QED tests, and the breaking of the Dirac degeneracy between the $2s$ and $2p_{1/2}$ states, the Lamb shift, will be discussed in some detail below. Along with the Lamb shift, corrections to the Dirac equation's prediction $g = 2$, first explained by *Schwinger* [3], are of central importance in QED. As bound state issues are emphasized here, we note only that this anomalous magnetic moment of the electron was first detected in hydrogen hyperfine splitting and Zeeman effect experiments, and that its present status is discussed in Chap. 29 "Tests of Fundamental Physics" in this volume along with a number of other extraordinarily high-precision tests of the theory.

It is the purpose of this chapter to discuss how the theory is applied to bound state problems. While almost every textbook on QFT describes the basic structure of QED, the applications given are usually to calculate scattering cross sections, the evaluation of one-loop radiative corrections, and the implementation of the renormalization program. The free electron propagator, which has a relatively simple form in momentum space, is used in the one-loop calculations. However, most of the precision tests of QED involve electrons that are bound, generally in a hydrogen-like atom. Even for the anomalous magnetic moment of the electron, which is calculated in terms of free Feynman diagrams, the electron is, in fact, bound in the constant magnetic field of a Penning trap [4]. While most QED effects require the evaluation of loop diagrams, these bound state calculations have rela-

J. R. Sapirstein (✉)
Department of Physics, University of Notre Dame
Notre Dame, IN, USA
e-mail: jsapirst@nd.edu

G.W.F. Drake (Ed.), *Springer Handbook of Atomic, Molecular, and Optical Physics*, Springer Handbooks,
https://doi.org/10.1007/978-3-030-73893-8_28

tively unfamiliar features that will be concentrated on here. It is, of course, important to test free QED with scattering experiments at the highest possible energies. To a large degree these tests have now merged with tests of the Standard Model. Experiments, for example, on electron–positron annihilation into muon or tau pairs have to include both the photon and the Z boson in the intermediate state along with a unified treatment of radiative corrections [5].

The fact that QED is part of the Standard Model affects bound states in two notable ways. Because of the weak interactions, parity nonconserving transitions become possible through Z boson exchange, as discussed elsewhere in this volume. The strong interactions, which in principle describe the nucleus of the bound state in terms of QCD, cannot yet provide precise predictions for charge radii and other nuclear properties. This leads to limitations on predictions for atomic structure. In this case, if QED is understood well enough, and accurate experiments are available, atomic spectroscopy can be used to obtain information about nuclear properties. At the time of this writing a prominent example of this is the case of muonic hydrogen, where measurements imply a smaller proton size than had been expected [6].

The Lamb shift in hydrogen is smaller than the atomic unit of energy (1 a.u. $= m_e c^2 \alpha^2$) by a factor α^3, under one part per million (ppm). For almost all electromagnetically bound states such a tiny correction is negligible compared to the uncertainty in the energy when solving the many-electron Schrödinger equation, $H\psi = E\psi$, where

$$H \equiv \sum_i^N \left(\frac{\boldsymbol{p}_i^2}{2m} - \frac{Z\alpha\hbar c}{r_i} \right) + \sum_{i>j=1}^N \frac{\hbar c\alpha}{|\boldsymbol{r}_i - \boldsymbol{r}_j|}$$
$$\psi = \psi(\boldsymbol{r}_1, \boldsymbol{r}_2, \ldots, \boldsymbol{r}_N) \,. \tag{28.1}$$

Solving for a particular bound state energy E_v this way we refer to as the Hamiltonian approach. For a single electron bound to any positively charged nucleus (which will be referred to as hydrogen for simplicity in what follows) this uncertainty is not present, and QED corrections are easily identified. For many-electron atoms, however, the electron–electron interaction term usually makes it too difficult to solve for E_v with the accuracy required to see such corrections. The techniques used to deal with the many-body problem are rather different from those used for QED corrections. While attempts to create a unified approach have been made [7], the most advanced atomic QED calculations have been carried out for hydrogen [8, 9]. To study QED in atoms with more than one electron accurate solutions to the structure problem are required, which are available for few electron atoms, particularly helium, and certain highly charged ions, as will be discussed below.

The Coulomb potential of the nucleus in Eq. (28.1),

$$V_C(r) \equiv -\frac{Z\alpha\hbar c}{r} \,, \tag{28.2}$$

is responsible for the dominant physics of binding. It is, thus, very useful to incorporate it into bound state QED calculations, which we will do here when we introduce Furry picture QED [10]. This is an example of an external field approximation [11]. Such approximations are very good for an electron in a classical electric or magnetic field, as a single electron has essentially no effect on the charge distributions and currents that create the external field. In an atom, the success of the Schrödinger equation shows that even a single nucleus effectively creates an external field. In this case, the fact that the nucleus is a single particle leads to observable corrections to the external field approximation. They are called recoil corrections, and if the nucleus is taken to have mass m_N, begin in order m/m_N. They vanish in the limit of infinite nuclear mass, which is called the nonrecoil limit.

The first QED treatments of recoil corrections were by *Salpeter* [12, 13], using the equation he had earlier derived with *Bethe* [14]. They formed a field theoretic function of the total energy of hydrogen E that had a pole at $E = E_v$, with recoil corrections identified as the difference of E_v with its nonrecoil limit.

This approach can also be used to calculate nonrecoil corrections in bound state QED, and the central purpose of this chapter is to show how this technique allows a unified treatment of both types of QED correction. The treatment also leads to a rigorous justification of the external field approximation for hydrogen.

Three central objects in the following are the electron propagator for one electron, the electron–nucleus propagator, and the many-electron propagator. While the terms propagator and Green function are basically synonymous, it is convenient to designate propagators as functions of time, and Green functions as time Fourier transforms depending on an energy E. We will show that the latter have poles when $E = E_v$ and develop perturbation theory for QED using this behavior. While QED has a Hamiltonian, the analysis that will be described here is based on the Green functions of the theory, and the approach is fundamentally different from the Hamiltonian approach. While for most bound state problems the Hamiltonian approach suffices, there are situations in which an approach grounded in field theory is absolutely necessary.

This chapter is organized as follows. In the next section free QED is set up in Coulomb gauge, and photon and electron propagators introduced. The perturbation expansion in the interaction picture is described, and the connection with Feynman gauge, which is particularly useful for calculating loop corrections, is shown.

In the next section, the Green functions for the free and bound electrons are formed as time Fourier transforms of the propagators, and the field theory based analog of Rayleigh–Schrödinger perturbation theory developed. The formulas for the one-loop electron self-energy and vacuum polarization

are derived and analyzed, and a short discussion of the two-loop Lamb shift is given.

In the following section, the approach is extended to electron–nucleus scattering, with emphasis placed on the emergence of the bound electron propagator in the limit of infinite nuclear mass. The perturbation theory for recoil corrections is described.

We then turn to the generalization of the method to many-electron atoms, and mention some applications of QED to highly charged many-electron ions. In the final section an alternative to the Bethe–Salpeter approach to recoil corrections is given, and remarks about nonrelativistic QED (NRQED) [15] are made.

28.2 Basic QED Formalism

In the following, we work in SI units, keeping all factors of $c, \hbar$, and ε_0. The photon momentum $\boldsymbol{q}$ is understood to be $\hbar$ times the associated wavenumber $\boldsymbol{k}$. The electron and proton charges are denoted q_e and q_p. The elementary charge e is understood to be positive, so $q_e = -e$ and $q_p = e$. In calculations, we will replace e^2 with $4\pi\hbar c\varepsilon_0\alpha$. The charge and mass of the nucleus are $q_N = Ze$ and m_N. Before treating bound states, we set up QED for free electrons. The electron field will be understood to describe either an electron or positron state, and the vacuum is the state with zero electrons, positrons, and photons, indicated by

$$\begin{aligned} b_s(\boldsymbol{p})|0\rangle &= 0 \\ d_s(\boldsymbol{p})|0\rangle &= 0 \\ a_\lambda(\boldsymbol{q})|0\rangle &= 0 \,. \end{aligned} \tag{28.3}$$

The destruction operators above have creation operator counterparts, and the only cases in which photon operators do not commute, or electron operators do not anticommute, are

$$\begin{aligned} [a_{\lambda_1}(\boldsymbol{q}_1), a^\dagger{}_{\lambda_2}(\boldsymbol{q}_2)] &= (2\pi)^3\delta_{\lambda_1\lambda_2}\delta^3(\boldsymbol{q}_1 - \boldsymbol{q}_2) \\ \{b_{s_1}(\boldsymbol{p}_1), b^\dagger{}_{s_2}(\boldsymbol{p}_2)\} &= \{d_{s_1}(\boldsymbol{p}_1), d^\dagger{}_{s_2}(\boldsymbol{p}_2)\} \\ &= (2\pi)^3\delta_{s_1 s_2}\delta^3(\boldsymbol{p}_1 - \boldsymbol{p}_2) \,. \end{aligned} \tag{28.4}$$

The electron field operator is given by

$$\begin{aligned} \psi(\boldsymbol{x}, t) = \int \frac{\mathrm{d}\boldsymbol{p}}{(2\pi)^3}\sqrt{\frac{mc^2}{E_p\hbar^3}}\sum_s \Big[& \mathrm{e}^{-\mathrm{i}p\cdot x/\hbar} b_s(\boldsymbol{p})u(\boldsymbol{p}, s) \\ & + \mathrm{e}^{\mathrm{i}p\cdot x/\hbar} d^\dagger(\boldsymbol{p})v(\boldsymbol{p}, s)\Big] \,, \end{aligned} \tag{28.5}$$

with $p\cdot x = E_p t - \boldsymbol{p}\cdot\boldsymbol{x}$, $E_p = \sqrt{(mc^2)^2 + c^2\boldsymbol{p}^2}$; $u(\boldsymbol{p}, s)$ and $v(\boldsymbol{p}, s)$ are Dirac spinors that form the projection operators

$$\Lambda_+(\boldsymbol{p}) \equiv \sum_s u(\boldsymbol{p}, s)\bar{u}(\boldsymbol{p}, s) = \frac{E_p\gamma_0 - c\boldsymbol{\gamma}\cdot\boldsymbol{p} + mc^2}{2E_p}$$

$$\Lambda_-(\boldsymbol{p}) \equiv \sum_s v(\boldsymbol{p}, s)\bar{v}(\boldsymbol{p}, s) = \frac{E_p\gamma_0 + c\boldsymbol{\gamma}\cdot\boldsymbol{p} - mc^2}{2E_p} \,. \tag{28.6}$$

The noncovariant normalization $u^\dagger(\boldsymbol{p}, s)u(\boldsymbol{p}, s') = \delta_{ss'}$, $v^\dagger(\boldsymbol{p}, s)v(\boldsymbol{p}, s') = \delta_{ss'}$ is used.

The charge density and current in terms of the electron field operators are

$$\begin{aligned} \rho(\boldsymbol{x}, t) &= \psi^\dagger(\boldsymbol{x}, t)\psi(\boldsymbol{x}, t) \\ \boldsymbol{j}(\boldsymbol{x}, t) &= \psi^\dagger(\boldsymbol{x}, t)\boldsymbol{\alpha}\psi(\boldsymbol{x}, t) \,. \end{aligned} \tag{28.7}$$

Normal ordering of the operators, in which destruction operators are moved to the right and creation to the left, is left implicit. The free electron Hamiltonian is

$$H_0(t) = \int \mathrm{d}\boldsymbol{x}\,\bar{\psi}(\boldsymbol{x}, t)[-\mathrm{i}\hbar c\boldsymbol{\alpha}\cdot\boldsymbol{\nabla} + mc^2\beta]\psi(\boldsymbol{x}, t) \,; \tag{28.8}$$

H_0 without t dependence indicated refers to the operator in square brackets.

Turning to the quantization of the electromagnetic field, as we use Coulomb gauge,

$$\boldsymbol{\nabla}\cdot\boldsymbol{A}(\boldsymbol{x}, t) = 0 \,. \tag{28.9}$$

This gives a constraint when quantizing $\boldsymbol{A}(\boldsymbol{x}, t)$, so that only the physical degrees of freedom of photons need be dealt with, and the field operator is

$$\begin{aligned} \boldsymbol{A}(\boldsymbol{x}, t) = \sqrt{\frac{1}{\hbar c\varepsilon_0}}\sum_{\lambda=1}^{2}\int \frac{\mathrm{d}\boldsymbol{q}}{(2\pi)^3\sqrt{2|\boldsymbol{q}|}} \\ \times\Big[a(\lambda, \boldsymbol{q})\hat{\varepsilon}_\lambda(\hat{q})\mathrm{e}^{-\mathrm{i}q\cdot x/\hbar} + a^\dagger(\lambda, \boldsymbol{q})\hat{\varepsilon}_\lambda(\hat{q})\mathrm{e}^{\mathrm{i}q\cdot x/\hbar}\Big] \,. \end{aligned} \tag{28.10}$$

The scalar potential, which is not quantized, is fixed by

$$\nabla^2\phi(\boldsymbol{x}, t) = -\frac{\rho(\boldsymbol{x}, t)}{\varepsilon_0} \,, \tag{28.11}$$

and the Hamiltonian describing the electrostatic energy is

$$\begin{aligned} H_C(t) = \frac{e^2}{8\pi\varepsilon_0}\int \mathrm{d}\boldsymbol{x}\int \mathrm{d}\boldsymbol{y} \\ \times\frac{\psi^\dagger(\boldsymbol{x}, t)\psi(\boldsymbol{x}, t)\psi^\dagger(\boldsymbol{y}, t)\psi(\boldsymbol{y}, t)}{|\boldsymbol{x} - \boldsymbol{y}|} \,. \end{aligned} \tag{28.12}$$

If the negative energy summation is removed from ψ, this Hamiltonian can be used to organize atomic many-body perturbation theory (MBPT) calculations [16]. Historically,

although QED was developed first, the power of the diagrammatic approach was later applied to many-electron atoms starting with the work of *Kelly* [17].

The remaining part of the interaction Hamiltonian comes from the minimal coupling replacement $c\boldsymbol{\alpha}\cdot\boldsymbol{p} \to c\boldsymbol{\alpha}\cdot(\boldsymbol{p} - q_e\boldsymbol{A}(\boldsymbol{x},t))$,

$$H_T(t) = -q_e c \int \mathrm{d}\boldsymbol{x}\, \boldsymbol{A}(\boldsymbol{x},t)\cdot\psi^\dagger(\boldsymbol{x},t)\boldsymbol{\alpha}\psi(\boldsymbol{x},t)\ , \quad (28.13)$$

where the subscript T stands for transverse.

The sum of $H_C(t)$ and $H_T(t)$ is the interaction Hamiltonian $H_I(t)$ and enters perturbation theory through its role in the time evolution operator $U(t_2,t_1)$. After transforming from the Schrödinger to the interaction picture through

$$|\psi_I(t)\rangle = \mathrm{e}^{\mathrm{i}H_0(t)t/\hbar}|\psi_S(t)\rangle\ , \quad (28.14)$$

it is given by

$$\begin{aligned} U(t_2,t_1) &= 1 + \frac{1}{\mathrm{i}\hbar}\int_{t_1}^{t_2}\mathrm{d}t H_I(t) + \left(\frac{1}{\mathrm{i}\hbar}\right)^2\int_{t_1}^{t_2}\mathrm{d}t \\ &\quad\times\int_{t_1}^{t}\mathrm{d}t' H_I(t)H_I(t') + \ldots \\ &= 1 + \frac{1}{\mathrm{i}\hbar}\int_{t_1}^{t_2}\mathrm{d}t H_I(t) + \frac{1}{2!}\left(\frac{1}{\mathrm{i}\hbar}\right)^2\int_{t_1}^{t_2}\mathrm{d}t \\ &\quad\times\int_{t_1}^{t_2}\mathrm{d}t' T(H_I(t)H_I(t')) + \ldots \\ &= T\left(\mathrm{e}^{\frac{1}{\mathrm{i}\hbar}\int_{t_1}^{t_2}\mathrm{d}t H_I(t)}\right)\ . \end{aligned} \quad (28.15)$$

Of particular importance is its value for $t_1 = -\infty, t_2 = \infty$, denoted S, and the matrix elements, the S-matrix,

$$\begin{aligned} S &\equiv U(\infty,-\infty) \\ S_{fi} &= \langle f|S|i\rangle\ . \end{aligned} \quad (28.16)$$

When one encounters the vacuum expectation value of a product of operators, a theorem due to Wick allows one to rearrange it in terms of creation and annihilation operators multiplying factors of the electron and photon propagators,

$$S_F(x,y) \equiv -\mathrm{i}\langle 0|T(\psi(\boldsymbol{x},t)\bar{\psi}(\boldsymbol{y},t'))|0\rangle \quad (28.17)$$

and

$$D^{ij}(x,y) \equiv -\mathrm{i}\langle 0|T(A^i(\boldsymbol{x},t)A^j(\boldsymbol{y},t'))|0\rangle\ . \quad (28.18)$$

Their form in momentum space is relatively simple,

$$S_F(x,y) = \frac{1}{\hbar^3}\int\frac{\mathrm{d}^4p}{(2\pi)^4}\frac{\mathrm{e}^{-\mathrm{i}p\cdot(x-y)/\hbar}}{p_0\gamma_0 - \vec{\gamma}\cdot\vec{p} - mc + \mathrm{i}\varepsilon}, \quad (28.19)$$

$$D^{ij}(x,y) = \frac{1}{\varepsilon_0\hbar c}\int\frac{\mathrm{d}^4q}{(2\pi)^4}\,\mathrm{e}^{-\mathrm{i}q\cdot(x-y)/\hbar}\frac{\left(\delta_{ij} - \frac{q_iq_j}{\boldsymbol{q}^2}\right)}{q_0^2 - \boldsymbol{q}^2 + \mathrm{i}\varepsilon}\ ; \quad (28.20)$$

$D^{ij}(x,y)$ is called the transverse photon propagator.

The compact form for $S_F(x,y)$ given above can be expanded into a form that separates positive and negative energy states,

$$\frac{1}{\not{p} - mc + \mathrm{i}\varepsilon} = \frac{\Lambda_+(\boldsymbol{p})}{p_0 - E_p/c + \mathrm{i}\varepsilon} + \frac{\Lambda_-(\boldsymbol{p})}{p_0 + E_p/c - \mathrm{i}\varepsilon}\ , \quad (28.21)$$

which will be used later.

If one wants the S-matrix for electron–electron scattering, for example, one chooses

$$\begin{aligned} |i\rangle &= b^\dagger(\boldsymbol{p}_1,s_1)b^\dagger(\boldsymbol{p}_2,s_2)|0\rangle \\ \langle f| &= \langle 0|b(\boldsymbol{p}_3,s_3)b(\boldsymbol{p}_4,s_4) \end{aligned} \quad (28.22)$$

(the states are properly antisymmetrized because the operators anticommute) and applies Wick's theorem. This procedure is greatly facilitated by a set of rules introduced by Feynman; they can be learned quickly, and correct QED matrix elements can be set up in an automatic way.

Unless the initial and final states are identical, the first contribution to S_{fi} comes from the term linear in H_C. Another term with the same number of factors q_e comes from the quadratic term with two H_T's. The latter involves a transverse photon propagator between the electrons. It is convenient to introduce a corresponding Coulomb photon propagator in order to rewrite the H_C term so that it also arises from a quadratic term. This can be done by including with D^{ij} another propagator, D^{00}. If one generalizes D^{ij} to $D^{\mu\nu}$, with $D^{0i} = D^{i0} = 0$ and

$$\begin{aligned} D^{00}(x,y) &= \frac{1}{\varepsilon_0\hbar c}\int\frac{\mathrm{d}^4q}{(2\pi)^4}\,\mathrm{e}^{-\mathrm{i}q\cdot(x-y)/\hbar}\frac{1}{\boldsymbol{q}^2} \\ &= \frac{\delta(t-t')}{4\pi\varepsilon_0|\boldsymbol{x}-\boldsymbol{y}|}\frac{\hbar}{c^2}\ , \end{aligned} \quad (28.23)$$

one reproduces S_{fi} by using

$$H_I(t) = q_e c\int\mathrm{d}\boldsymbol{x}\, A^\mu(\boldsymbol{x},t)\bar{\psi}(\boldsymbol{x},t)\gamma^\mu\psi(\boldsymbol{x},t) \quad (28.24)$$

and using the photon propagator in Coulomb gauge described above.

This simpler form for $H_I(t)$ comes at the apparent cost of the more complicated photon propagator just described, but the photon propagator is always encountered in the form $A_\mu(q)D^{\mu\nu}B_\nu(q)$. If one requires $q^\mu A_\mu = 0$ and $q^\mu B_\mu = 0$, a short calculation shows

$$\frac{A_0B_0}{\boldsymbol{q}^2} + \frac{\boldsymbol{q}^2\boldsymbol{A}\cdot\boldsymbol{B} - \boldsymbol{A}\cdot\boldsymbol{q}\,\boldsymbol{B}\cdot\boldsymbol{q}}{\boldsymbol{q}^2(q_0^2 - \boldsymbol{q}^2)} = -\frac{A_0B_0 - \boldsymbol{A}\cdot\boldsymbol{B}}{q_0^2 - \boldsymbol{q}^2} = -\frac{A_\mu B_\nu g^{\mu\nu}}{q^2}\,, \tag{28.25}$$

where we will suppress the $\mathrm{i}\varepsilon$ in the following for brevity. Because of this one can use the simpler Feynman gauge propagator

$$D_F^{\mu\nu}(x,y) = \frac{1}{\hbar c\varepsilon_0}\int\frac{\mathrm{d}^4q}{(2\pi)^4}\,\mathrm{e}^{-\mathrm{i}q\cdot(x-y)/\hbar}\frac{-g^{\mu\nu}}{q^2}\,. \tag{28.26}$$

The requirement that $A^\mu q_\mu = B^\mu q_\mu = 0$ can be shown to be satisfied as long as a gauge invariant set of diagrams are evaluated together. In the following, we will use both gauges: Coulomb gauge is useful for recoil calculations and Feynman gauge for calculations involving loops with ultraviolet divergences.

In cases when a fixed external electromagnetic potential is present, one would decompose

$$A^\mu(x) \to A^\mu_{\mathrm{ext}}(x) + A^\mu(x)\,, \tag{28.27}$$

quantizing only the second term. This is the external field approximation [11]. The part of H_I involving the external field can then be grouped with $H_0(t)$ so that, restricting our attention to external fields constant in time,

$$H_0(t) = \int\mathrm{d}\boldsymbol{x}\,\psi^\dagger(\boldsymbol{x},t)\big[-\mathrm{i}\hbar c\boldsymbol{\alpha}\cdot\boldsymbol{\nabla} - q_e c\boldsymbol{\alpha}\cdot\boldsymbol{A}_{\mathrm{ext}}(\boldsymbol{x}) + mc^2\beta + V(\boldsymbol{x})\big]\psi(\boldsymbol{x},t)\,, \tag{28.28}$$

with $q_e A^0{}_{\mathrm{ext}}(\boldsymbol{x}) = V(\boldsymbol{x})$. If the removal of the quantized part of H_I is carried out in this case, the interaction picture is referred to as the Furry picture [10]. This form of QED is extremely useful, as it builds in the dominant physics of binding, although at the cost of a more complicated electron propagator.

In Furry picture QED, the photon propagator is unchanged, but the electron propagator now depends on both $\boldsymbol{x}$ and $\boldsymbol{y}$ rather than only on their difference. We distinguish the free electron propagator $S_F(x,y)$ from the bound propagator by including a suffix V, and define the related Green function through

$$S_F^V(x,y) = \int\frac{\mathrm{d}E}{2\pi}\mathrm{e}^{-\mathrm{i}E(t-t')/\hbar}G(E,\boldsymbol{x},\boldsymbol{y})\gamma_0\,. \tag{28.29}$$

When $V(\boldsymbol{r})$ is the Coulomb potential, we call $S_F^V(x,y)$ the Coulomb propagator, and $G(E,\boldsymbol{x},\boldsymbol{y})$ the Coulomb Green function. In general, the Green function satisfies

$$[E - (H_0 + V(\boldsymbol{x}))]G(E,\boldsymbol{x},\boldsymbol{y}) = \delta^3(\boldsymbol{x}-\boldsymbol{y})\,. \tag{28.30}$$

All information about the energy eigenvalues and eigenfunctions is contained in $G(E,\boldsymbol{x},\boldsymbol{y})$. This is most clearly seen when it is represented as a spectral decomposition,

$$G(E,\boldsymbol{x},\boldsymbol{y}) = \sum_m\frac{\psi_m(\boldsymbol{x})\psi_m^\dagger(\boldsymbol{y})}{E - \varepsilon_m(1-\mathrm{i}\delta)}\,. \tag{28.31}$$

In this form, one identifies the eigenvalues ε_m as the position of simple poles of E, with the eigenvectors associated with the residue of the pole. (If there is a continuous distribution of energies, the pole is replaced with a branch cut.)

To isolate a particular pole $m = v$, we form the projection

$$G_{vv}(E) \equiv \int\mathrm{d}\boldsymbol{x}\int\mathrm{d}\boldsymbol{y}\,\psi_v{}^\dagger(\boldsymbol{x})G(E,\boldsymbol{x},\boldsymbol{y})\psi_v(\boldsymbol{y})\,, \tag{28.32}$$

which collapses the sum over m in the spectral decomposition, giving

$$G_{vv}(E) = \frac{1}{E-\varepsilon_v}\,. \tag{28.33}$$

The related identities

$$\int\mathrm{d}\boldsymbol{x}\,\psi_v{}^\dagger(\boldsymbol{x})G(E,\boldsymbol{x},\boldsymbol{y}) = \frac{1}{E-\varepsilon_v}\psi_v^\dagger(\boldsymbol{y})$$
$$\int\mathrm{d}\boldsymbol{y}\,G(E,\boldsymbol{x},\boldsymbol{y})\psi_v(\boldsymbol{y}) = \frac{1}{E-\varepsilon_v}\psi_v(\boldsymbol{x}) \tag{28.34}$$

will also be used.

For the free case, we denote the Green function as $G_0(E,\boldsymbol{x},\boldsymbol{y})$. It satisfies Eq. (28.30) with $V = 0$, and a useful representation of it is

$$G_0(E,\boldsymbol{x},\boldsymbol{y}) = \frac{1}{\hbar^3}\int\frac{\mathrm{d}\boldsymbol{p}}{(2\pi)^3}\frac{\mathrm{e}^{\mathrm{i}\boldsymbol{p}\cdot(\boldsymbol{x}-\boldsymbol{y})/\hbar}}{E\gamma_0 - c\boldsymbol{\gamma}\cdot\boldsymbol{p} - mc^2 + \mathrm{i}\varepsilon}\gamma_0\,. \tag{28.35}$$

The two functions are related by

$$G(E,\boldsymbol{x},\boldsymbol{y}) = G_0(E,\boldsymbol{x},\boldsymbol{y}) + \int\mathrm{d}\boldsymbol{r}\,G_0(E,\boldsymbol{x},\boldsymbol{r})V(\boldsymbol{r})G(E,\boldsymbol{r},\boldsymbol{y})\,, \tag{28.36}$$

which leads to the expansion

$$G(E,\boldsymbol{x},\boldsymbol{y}) = G_0(E,\boldsymbol{x},\boldsymbol{y}) + \int \mathrm{d}\boldsymbol{r}_1 G_0(E.\boldsymbol{x},\boldsymbol{r}_1)V(\boldsymbol{r}_1)G_0(E,\boldsymbol{r}_1,\boldsymbol{y}) + \int \mathrm{d}\boldsymbol{r}_1 \int \mathrm{d}\boldsymbol{r}_2 G_0(E,\boldsymbol{x},\boldsymbol{r}_1)V(\boldsymbol{r}_1) \times G_0(E,\boldsymbol{r}_1,\boldsymbol{r}_2)V(\boldsymbol{r}_2)G_0(E,\boldsymbol{r}_2,\boldsymbol{y}) + \ldots \tag{28.37}$$

A characteristic difficulty of the atomic bound state problem is that going to the next order in the expansion of $G(E,\boldsymbol{x},\boldsymbol{y})$ does not always lead to additional powers of α. Each term is nominally of the same order, and in many cases, the series must be summed to all orders. However, the expansion remains very useful. One reason for this is that the ultraviolet divergences of QED are generally associated with the first and second terms of the expansion, and isolating them allows manipulations to simplify loop calculations. As those are carried out in momentum space, we will need the momentum space version of the expansion of Eq. (28.37),

$$G(E,\boldsymbol{p},\boldsymbol{q})\gamma_0 = \hbar^3\Bigg[\frac{(2\pi)^3\delta^3(\boldsymbol{p}-\boldsymbol{q})}{E\gamma_0 - c\boldsymbol{\gamma}\cdot\boldsymbol{p} - mc^2} + \frac{1}{E\gamma_0 - c\boldsymbol{\gamma}\cdot\boldsymbol{p} - mc^2}\gamma_0\frac{4\pi Z\alpha c}{|\boldsymbol{p}-\boldsymbol{q}|^2} \times \frac{1}{E\gamma_0 - c\boldsymbol{\gamma}\cdot\boldsymbol{q} - mc^2} + \frac{1}{E\gamma_0 - c\boldsymbol{\gamma}\cdot\boldsymbol{p} - mc^2}\gamma_0\int\frac{\mathrm{d}\boldsymbol{k}}{(2\pi)^3} \times \frac{4\pi Z\alpha c}{|\boldsymbol{p}-\boldsymbol{k}|^2}\frac{1}{E\gamma_0 - c\boldsymbol{\gamma}\cdot\boldsymbol{p} - mc^2} \times \gamma_0\frac{4\pi Z\alpha c}{|\boldsymbol{k}-\boldsymbol{q}|^2}\frac{1}{E\gamma_0 - c\boldsymbol{\gamma}\cdot\boldsymbol{q} - mc^2} + \ldots\Bigg]. \tag{28.38}$$

An interesting feature of the Furry picture is the role of negative energy states for many electron atoms. For free electrons, the unitary transformation to the interaction picture is unambiguous, chosen to subtract H_I, and the spinors $u(\boldsymbol{p},s)$ and $v(\boldsymbol{p},s)$ that enter the electron field operator are also unique. For hydrogen, the solutions are solutions to the Dirac equation in a Coulomb field, which are also unambiguous. However, for many electron atoms, an extended Furry representation can be used in order to account for some portion of electron screening, and this can be done using any local potential $U(\boldsymbol{x})$. This extension involves introducing an additional interaction Hamiltonian,

$$H_I'(t) = -\int \mathrm{d}\boldsymbol{x}\, U(\boldsymbol{x})\psi^\dagger(\boldsymbol{x},t)\psi(\boldsymbol{x},t) \tag{28.39}$$

along with changing $V(\boldsymbol{x}) \to V(\boldsymbol{x}) + U(\boldsymbol{x})$ in Eq. (28.28), and will be used when we discuss many-electron calculations. The positive and negative energy solutions to the Dirac equation now depend on the choice of the screening potential. For the positive energy solutions, one then faces the same problem as in the Hamiltonian approach. Except for atoms with only a few electrons, the only practical way to even form a wave function is to assume that all electrons move in the same potential, so that a lowest order approximation of the wave function as a Slater determinant of occupied states can be formed. When the potential is modified to incorporate screening, a modification of the Furry picture leads to a replacement of the Coulomb potential with the screened potential, as will be discussed later. The associated negative energy states also depend on the potential, so that forming a general projection operator to remove them, a useful approximation in relativistic many body physics, is problematical.

28.3 Perturbation Theory with Green Functions

We now introduce the basic approach to calculating energy levels in QED, which is to form a function of an energy E that has poles at the eigenvalue E_v. We first generalize the lowest order electron propagator that we have been dealing with to its exact form. This is done by starting in Heisenberg representation, defining

$$S_2(x,y) = \langle 0|T(\psi_H(x)\bar{\psi}_H(y))|0\rangle\ , \tag{28.40}$$

sometimes referred to as the two-point function. We then define the associated Green function,

$$G_2(E,\boldsymbol{x},\boldsymbol{y}) = -\frac{\mathrm{i}}{\hbar}\int \mathrm{d}t\, \mathrm{e}^{\mathrm{i}Et/\hbar} \times \langle 0|T(\psi_H(\boldsymbol{x},t)\bar{\psi}_H(\boldsymbol{y},0))|0\rangle \mathrm{e}^{-\varepsilon|t|/\hbar}\ . \tag{28.41}$$

We have set $t' = 0$ and introduced a convergence factor with the understanding that the limit $\varepsilon \to 0$ is to be taken.

We next note that a positive energy state ψ_v that satisfies $H\psi_v = E_v\psi_v$ leads to a pole at $E = E_v$ once the integral over positive values of t is carried out. This is because for such values the operators are already time ordered, and a complete set of states can be inserted between them, so that

$$G_2(E,\boldsymbol{x},\boldsymbol{y}) = -\frac{\mathrm{i}}{\hbar}\sum_m \int_0^\infty \mathrm{d}t\, \mathrm{e}^{-\varepsilon t/\hbar}\mathrm{e}^{\mathrm{i}Et/\hbar} \times \langle 0|\psi_H(\boldsymbol{x},t)|m\rangle\langle m|\psi_H(\boldsymbol{y},0)|0\rangle$$

$$= -\frac{\mathrm{i}}{\hbar}\sum_m \int_0^\infty \mathrm{d}t\, \mathrm{e}^{\mathrm{i}t(E-E_m+\mathrm{i}\varepsilon)/\hbar} \times \langle 0|\psi_H(\boldsymbol{x},0)|m\rangle\langle m|\bar{\psi}(\boldsymbol{y},0)|0\rangle \ . \quad (28.42)$$

We have used

$$\psi_H(\boldsymbol{x},t) = \mathrm{e}^{\mathrm{i}Ht/\hbar}\psi_H(\boldsymbol{x},0)\mathrm{e}^{-\mathrm{i}Ht/\hbar} \quad (28.43)$$

to remove the time dependence from the electron field operator. This makes it possible to carry out the t integration, so for a particular state v

$$G_2(E,\boldsymbol{x},\boldsymbol{y}) \approx \frac{1}{E-E_v+\mathrm{i}\varepsilon} \ . \quad (28.44)$$

We now have a way of finding E_v through the analysis of $G_H(E,\boldsymbol{x},\boldsymbol{y})$, an object that is well defined in field theory. Of course, determining E_v is tantamount to exactly solving QED, so in practice, some kind of perturbation expansion must be made. Going to interaction representation allows the expansion to be derived through expanding the time evolution operator. However, while Feynman diagrams can be used for the expansion, instead of generating S-matrix elements we will find modifications of the Green function involving double poles, and the energy shifts will be the factors multiplying them. An extremely thorough treatment of this approach is given by *Shabaev* in [18]. The basic idea follows by considering the second term in the Taylor expansion of

$$\frac{1}{E-\varepsilon_v-\delta E_v} = \frac{1}{E-\varepsilon_v} + \frac{\delta E_v}{(E-\varepsilon_v)^2} + \ldots \quad (28.45)$$

The third term in the expansion will give a term with a triple pole, and so on, but to generalize first-order Rayleigh–Schrödinger perturbation theory to field theory it suffices to find terms with double poles and identify the factor with δE_v. As emphasized by *Yennie* [19], this approach to QED perturbation theory allows one to examine a limited set of Feynman diagrams contributing to a Green function. To find the shift of a state $\psi_v(\boldsymbol{x})$ with energy ε_v, one projects out that state as described above Eq. (28.33), and reads off the energy shift from coefficients of $1/(E-\varepsilon_v)^2$.

Transforming from the Heisenberg to the interaction representation is done by including a factor of $U(\infty,-\infty)$ in the two-point function and dividing by the vacuum expectation value,

$$S_2(x,y) = \frac{\langle 0|T(U\psi(\boldsymbol{x},t)\bar{\psi}(\boldsymbol{y},0))|0\rangle}{\langle 0|U|0\rangle} \ . \quad (28.46)$$

The denominator term eliminates contributions involving disconnected diagrams. We have already shown in Eq. (28.33) that in lowest order, the projected Green function has a pole at the Dirac energies ε_v. In particular, the $2s$ and $2p_{1/2}$ are degenerate. The experimental measurement of the energy difference of the state by *Lamb* and *Retherford* [20] was an important impetus for developing methods to calculate δE_v.

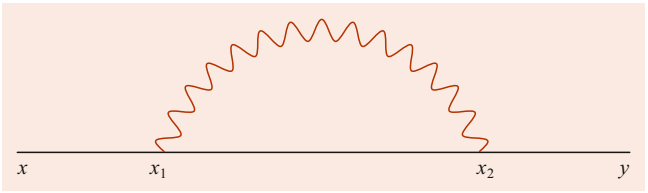

Fig. 28.1 The Green function for one-loop self-energy

The first nonvanishing term in the Taylor expansion when using Feynman gauge is from second order, as one needs at least a pair of photon fields to combine into a propagator. The six electron fields contract into three propagators in two topologies, the self-energy (SE) and vacuum polarization (VP). We start with the self-energy, shown in Fig. 28.1.

$$G_{SE}(E) = -\frac{\mathrm{i}}{\hbar}\int\frac{\mathrm{d}E}{2\pi}\mathrm{e}^{\mathrm{i}Et/\hbar}\left(\frac{q_e c}{\hbar}\right)^2\int\mathrm{d}x_2\int\mathrm{d}x_1 \times S_F^V(x,x_1)\gamma_\mu S_F^V(x_1,x_2)\gamma_\nu S_F^V(x_2,y) \times {D_F}^{\mu\nu}(x_1,x_2) \ . \quad (28.47)$$

The "outside" propagators $S_F^V(x,x_1)$ and $S_F^V(x_2,y)$ are next replaced with integrals over the variables E_1 and E_3 of $G(E_1,\boldsymbol{x},\boldsymbol{x}_1)$ and $G(E_3,\boldsymbol{x}_2,\boldsymbol{y})$ using Eq. (28.29), and represented as spectral decompositions as in Eq. (28.31). The interior Green function is written as an integral over E_2 of $G(E_2,\boldsymbol{x}_2,\boldsymbol{x}_1)$ and left in that form. We collapse the sums as described earlier. The integral over t involves only $S(x,x_1)$, and carrying it out gives a delta function that puts $E_1 = E$. The remaining integrals over t_1 and t_2 force $E_3 = E$ and $E_2 = E - cq_0$, and we have a double pole term,

$$G_{SE}(E)_{vv} = -\frac{1}{(E-\varepsilon_v)^2}\frac{\mathrm{i}e^2}{\varepsilon_0}\frac{c}{\hbar}\int\mathrm{d}\boldsymbol{x}\mathrm{d}\boldsymbol{y} \times \int\frac{\mathrm{d}^4q}{(2\pi)^4}\frac{\mathrm{e}^{\mathrm{i}\boldsymbol{q}\cdot(\boldsymbol{x}-\boldsymbol{y})/\hbar}}{q^2+\mathrm{i}\delta}\bar{\psi}_v(\boldsymbol{x})\gamma_\mu \times G(E-cq_0,\boldsymbol{x},\boldsymbol{y})\gamma_0\gamma^\mu\psi_v(\boldsymbol{y}) \ . \quad (28.48)$$

The factor multiplying the double pole is identified with the self-energy part of the one-loop Lamb shift,

$$E_{SE}^{(2)} = -4\pi\mathrm{i}\alpha c^2\int\mathrm{d}\boldsymbol{x}\mathrm{d}\boldsymbol{y}\int\frac{\mathrm{d}^4q}{(2\pi)^4}\frac{\mathrm{e}^{\mathrm{i}\boldsymbol{q}\cdot(\boldsymbol{x}-\boldsymbol{y})/\hbar}}{q^2+\mathrm{i}\delta} \times \bar{\psi}_v(\boldsymbol{x})\gamma_\mu G(\varepsilon_v-cq_0,\boldsymbol{x},\boldsymbol{y})\gamma_0\gamma^\mu\psi_v(\boldsymbol{y}) \ , \quad (28.49)$$

where we have replaced E with ε_v in the numerator of G.

Because the integral over q is ultraviolet infinite, $E_{SE}^{(2)}$ is not defined as it stands. If the d^4q integral were Euclidean, the radial part of the integral would go as q^3dq: the denominator at large q goes as q^3, so it is nominally linearly divergent. Before meaningful results can be calculated, two steps are needed: regularization and renormalization. Regularization involves making the integral a finite quantity, for example by cutting the q integral off at a large momentum Λ. Renormalization then involves showing that terms that diverge when Λ goes to infinity have the effect of changing quantities like the electron mass and charge. In a renormalizable theory such as QED, a limited number of renormalizations lead to finite results, with residual terms depending on the regularization vanishing in the limit.

An important breakthrough made in QED, which had basically been stalled for years by these infinities, was the realization they were present for both free and bound electrons. To show this, it is useful to present the self-energy term in momentum space,

$$E_{SE}^{(2)} = -\frac{4\pi i\alpha c^2}{\hbar^6}\int\frac{\mathrm{d}^4q}{(2\pi)^4}\frac{1}{q^2}\int\frac{\mathrm{d}\boldsymbol{p}_2}{(2\pi)^3}\int\frac{\mathrm{d}\boldsymbol{p}_1}{(2\pi)^3} \times\bar{\psi}_v(\boldsymbol{p}_2)\gamma_\mu G(\varepsilon_v - cq_0, \boldsymbol{p}_2 - \boldsymbol{q}, \boldsymbol{p}_1 - \boldsymbol{q}) \times\gamma_0\gamma^\mu\psi_v(\boldsymbol{p}_1) \tag{28.50}$$

and examine the first two terms in the expansion of the Green function given in Eq. (28.38).

Introducing a four-vector $p = (\varepsilon_v/c, \boldsymbol{p})$, the first term, the "zero potential" or OP term, can be written as

$$E_{0P}^{(2)} = \frac{1}{\hbar^3}\int\frac{\mathrm{d}\boldsymbol{p}}{(2\pi)^3}\bar{\psi}_v(\boldsymbol{p})\Sigma(p)\psi_v(\boldsymbol{p})\,, \tag{28.51}$$

where

$$\Sigma(p) = -4\pi i\alpha\int\frac{\mathrm{d}^4q}{(2\pi)^4}\frac{1}{q^2}\gamma_\mu \times\frac{(\varepsilon_v - cq_0)\gamma_0 - c\boldsymbol{\gamma}\cdot(\boldsymbol{p}-\boldsymbol{q}) + mc^2}{(q-p)^2 - m^2c^2}\gamma^\mu\,, \tag{28.52}$$

and the identity

$$\frac{1}{\not{p} - mc} = \frac{\not{p} + mc}{p^2 - m^2c^2} \tag{28.53}$$

has been used. (If, instead, Eq. (28.21) is used for the electron propagator, it can be shown that there is a linear divergence present in the two parts that cancels.) We proceed by combining the denominators using

$$\frac{1}{AB} = \int_0^1 \mathrm{d}x\frac{1}{(Ax + B(1-x))^2} \tag{28.54}$$

and find

$$\Sigma(p) = -4\pi i\alpha c\int\frac{\mathrm{d}^4q}{(2\pi)^4}\int_0^1\mathrm{d}x \times\frac{\gamma_\mu(\gamma\cdot(p-q) + mc)\gamma^\mu}{[(q-xp)^2 - xm^2c^2(1-(1-x)p^2/(mc)^2)]^2}\,. \tag{28.55}$$

In this form, it is not hard to see that the divergence is logarithmic: the linear divergence, associated with the factor $\not{q}$, vanishes by symmetry after transforming $q \to q + xp$.

A powerful technique to regulate these infinities is dimensional regularization [21], where $d^4q \to dq_0d^rq$, with $r = 3 - \varepsilon$. With ε small but nonzero, the integrals above can be done after transforming to a Euclidean form through $q_0 \to iq_4$. After defining a constant $C \equiv (4\pi)^{\varepsilon/2}\Gamma(1+\varepsilon/2)$ and then expanding the result to order ε^0, one has

$$\Sigma(p) = \frac{\alpha}{\pi}\left(\frac{3C}{2\varepsilon} + 1\right)mc^2 - \frac{\alpha}{2\pi}\left(\frac{C}{\varepsilon} + 1\right)(c\not{p} - mc^2) - \frac{\alpha}{4\pi}\int\mathrm{d}x\ln(1-(1-x)p^2/(mc)^2) \times[mc^2(1+x) - (1-x)(c\not{p} - mc^2)]\,. \tag{28.56}$$

For an on-shell free electron, only the first term survives and is termed the second-order electron self-mass, $\delta m^{(2)}$. It has the effect of shifting the electron mass from m to $m + \delta m^{(2)}$. This is to be identified with the observed mass of the electron, so if we use the observed mass in propagators, a renormalization counterterm must be included in the interaction Hamiltonian.

For a bound electron, the counterterm also removes the divergent self-mass term. The realization that a renormalization process that accounted for the changed meaning of the mass of free electrons would remove a divergence of bound electrons was a crucial step in establishing the modern form of QED. However, a divergence still remains for hydrogen. It is also removed by another renormalization, but because of an identity associated with current conservation, also directly cancels with a divergence from another part of the self-energy, the one-potential (1P) term.

The 1P term comes from the second term in Eq. (28.37), which is represented by the vertex diagram shown in Fig. 28.3. If we now define the two four-vectors $p_1 = (\varepsilon_v/c, \boldsymbol{p}_1)$ and $p_2 = (\varepsilon_v/c, \boldsymbol{p}_2)$, this part of the self-energy is

$$E_{1P}^{(2)} = \frac{1}{\hbar^3}\int\frac{\mathrm{d}\boldsymbol{p}_2}{(2\pi)^3}\frac{\mathrm{d}\boldsymbol{p}_1}{(2\pi)^3}\bar{\psi}_v(\boldsymbol{p}_2)\Gamma_0(p_2, p_1) \times\psi_v(\boldsymbol{p}_1)\frac{4\pi Z\alpha c}{|\boldsymbol{p}_2 - \boldsymbol{p}_1|^2}\,, \tag{28.57}$$

with

$$\Gamma_\rho(p_2, p_1) = -4\pi i\alpha \int \frac{d^4q}{(2\pi)^4}\frac{1}{q^2}\gamma^\mu \frac{1}{\not p_1 - \not q - mc} \times \gamma_\rho \frac{1}{\not p_2 - \not q - mc}\gamma^\mu \,. \tag{28.58}$$

As with $\Sigma(p)$, $\Gamma_\rho(p_2, p_1)$, the one-loop vertex, is a standard one-loop expression that can be evaluated independently of the bound state problem. When it is sandwiched between on-shell electron wave functions, it can be expressed in terms of two form factors,

$$\Gamma_\rho(p_2, p_1) = \gamma_\rho F_1(q^2) + F_2(q^2)\frac{i\sigma^{\rho\nu}q_\nu}{2mc} \,, \tag{28.59}$$

where $q = p_2 - p_1$. Note that $q^2 = -|\boldsymbol{p}_2 - \boldsymbol{p}_1|^2$. While we will concentrate on $F_1(q^2)$, we note that $F_2(q^2)$ goes to $\alpha/2\pi$ when q is small compared to mc, which is the case for atomic momenta. This gives a contribution to the leading order Lamb shift, and in the case of the external field being a magnetic field gives the Schwinger correction [3].

The $F_1(q^2)$ has two divergences, the first being the same kind of ultraviolet divergence that dimensional regularization controls, and the second an infrared divergence. Although there is no infrared divergence in $E^{(2)}_{1P}$, the requirement of being on shell induces one in $F_1(q^2)$. For small values of q, one has

$$F_1(q^2) = \frac{\alpha}{2\pi}\left(\frac{C}{\varepsilon} + 1\right) + \frac{\alpha}{3\pi}\frac{q^2}{(mc)^2}\left(\ln\frac{mc^2}{\varepsilon} - \frac{3}{8}\right) , \tag{28.60}$$

where ε is a lower cutoff energy used to regulate the infrared divergence. The ultraviolet divergence can be seen to cancel with the 0P term after using the Dirac equation.

After noting the cancelation of the ultraviolet divergences, while the calculation of this term can be carried out numerically, one can immediately determine important properties of the energy shift by considering the form given above. In particular, the term of order q^2 in F_1, when put into $E^{(2)}_{1P}$, leads to a factor of the wave function at the origin squared, as the $\boldsymbol{p}_1$ and $\boldsymbol{p}_2$ integrations are decoupled and can be carried out separately. Using the nonrelativistic form, this leads to a logarithmic term

$$E^{(2)}_{1P} \approx \frac{mc^2\alpha(Z\alpha)^4}{\pi n^3}\frac{4}{3}\ln\frac{mc^2}{\varepsilon} \,. \tag{28.61}$$

The factor multiplying $4/3\,\ln mc^2/\varepsilon$ characterizes the basic size of the Lamb shift. Compared to the scale of Bohr energies, $mc^2(Z\alpha)^2$, the effect is suppressed by a factor $\alpha(Z\alpha)^2$; while less than a ppm effect at low Z, it can be of order of a percent at high Z, as will be discussed later.

If the replacement $\varepsilon \to m(Z\alpha)^2$ is made, the cutoff form factor term gives, for s-states,

$$\Delta E = \frac{mc^2\alpha(Z\alpha)^4}{\pi n^3}\frac{4}{3}\ln(Z\alpha)^{-2} \,, \tag{28.62}$$

the largest contribution, at 1334.801 MHz, to the Lamb shift in hydrogen. As the measurement is about 1057 MHz, the constant term is also important. It involves energies less than the cutoff and is sensitive to atomic structure. It receives contributions from each term in the expansion of the propagator we have been using, but the sum of the terms, the Bethe logarithm, can be numerically evaluated to high precision [22].

While the lowest order contribution to the self-energy, of order $mc^2\alpha(Z\alpha)^4$, is understood, it is corrected by powers of $Z\alpha$ along with logarithms of $Z\alpha$, referred to as binding corrections. While the difficulty of the calculations increases as the power increases, they have been carried out to the high orders described elsewhere. However, for high Z this approach breaks down, and a numerical calculation is needed. For this reason, we now turn to a discussion of these calculations. We note, however, the useful constraint of requiring that the numerical methods, which work at any value of Z (although the numerical difficulty increases as Z gets small), agree with the power series expansion at low Z.

While the program began in 1955 [23, 23], numerical control to high accuracy was only relatively recently achieved. To set the calculations up, one first carries out the $d\boldsymbol{q}$ integration and does the Wick rotation $q_0 \to iu/c$ in Eq. (28.49). Both the Coulomb Green function and the photon Green function are expanded in partial waves. Using spherical symmetry allows the four angle integrations to be done, leaving a sum over partial waves of a three-dimensional integral. The main difficulty for the numerical approach is the fact the summation over partial waves extends to infinity. The most accurate values have been presented in [25], where acceleration techniques are used to extrapolate the sum to infinity, after which the radial and energy integrals are done. Highly accurate results have been presented for the $n = 1$ and $n = 2$ states for all Z in [26]. In this case, the integrations are carried out before the partial wave expansion, but subtraction techniques, to be discussed below, are used to make the partial wave expansion converge very rapidly, so that fewer than 20 terms are needed [27].

All numerical approaches involve subtractions, which are done in a number of ways. We have already examined the first and second terms in Eq. (28.37). The finite terms left over after the ultraviolet divergent terms have been canceled can be accurately evaluated, so if we add and subtract $E^{(2)}_{0P} + E^{(2)}_{1P}$ from the one-loop self-energy but express the subtracted part in coordinate space, we have an ultraviolet finite coordinate space term to deal with called the many-potential (MP) term. It is called this since only the second-order and higher

terms in Eq. (28.37) remain after the subtraction. This approach was suggested by *Blundell* and *Snyderman* [28] and has been used extensively.

This procedure involves subtracting, using a shorthand notation for the second term in Eq. (28.37), G_0VG_0. Originally, however, *Mohr* [29] instead subtracted a term $G_0\bar{V}G_0$, where, undoing the shorthand notation,

$$G_0\bar{V}G_0 = \frac{V(x_2)+V(x_1)}{2} \times \int \mathrm{d}\boldsymbol{w}\, G_0(E,\boldsymbol{x}_2,\boldsymbol{w})G_0(E,\boldsymbol{w},\boldsymbol{x}_1)\,. \quad (28.63)$$

The integral over $\boldsymbol{w}$ can be carried out using

$$\begin{aligned}&\int \mathrm{d}\boldsymbol{w}\, G_0(E,\boldsymbol{x}_2,\boldsymbol{w})G_0(E,\boldsymbol{w},\boldsymbol{x}_1)\\ &= \int \mathrm{d}\boldsymbol{w} \sum_m \frac{\psi_m(\boldsymbol{x}_2)\psi_m^\dagger(\boldsymbol{w})}{E-\varepsilon_m} \sum_n \frac{\psi_n(\boldsymbol{w})\psi_n^\dagger(\boldsymbol{x}_1)}{E-\varepsilon_n}\\ &= \sum_m \frac{\psi_m(\boldsymbol{x}_2)\psi_m^\dagger(\boldsymbol{x}_1)}{(E-E_m)^2}\\ &= -\frac{\mathrm{d}}{\mathrm{d}E} G_0(E,\boldsymbol{x}_2,\boldsymbol{x}_1)\,, \end{aligned} \quad (28.64)$$

and a much simpler function results. This allowed the first accurate calculations of the self-energy for a range of Z [29]. The argument just given for two Green functions applies to the product of any number of them, resulting in successively higher derivatives of a single Green function. This was used in [27] to form the subtractions mentioned above.

A set of corrections to the self-energy arise when it is perturbed that illustrate other aspects of the Green function perturbation theory expansion [30–32]. These corrections must be evaluated, for example, when dealing with radiative corrections to the Zeeman effect. For laboratory magnetic fields, the energy shift of a bound electron in an atom, E_Z, need be treated only in first order. However, to include the effect of the one-loop self-energy (which in the nonrelativistic case is dominated by the Schwinger correction), one must treat the diagrams of both figures (Figs. 28.2 and 28.3). (For Fig. 28.2, the Green functions are understood to be $G(z,\boldsymbol{x},\boldsymbol{y})$ rather than $G_0(z,\boldsymbol{x},\boldsymbol{y})$, and the vertical photon line as the magnetic field rather than the Coulomb field of the proton.) The latter diagrams have four electron propagators. We recall that for the one-loop self-energy, one of the three propagators was not decomposed, and the other two gave a double pole.

The same arguments apply to Fig. 28.2, and one leaves both interior propagators unexpanded. For the diagrams of Fig. 28.3, one encounters terms involving $\Sigma(p)$, but with argument E not replaced with ε_v, sandwiched with various states. Because only one propagator is left "as is", there is a triple pole at $E=\varepsilon_v$. The triple pole itself gives no new

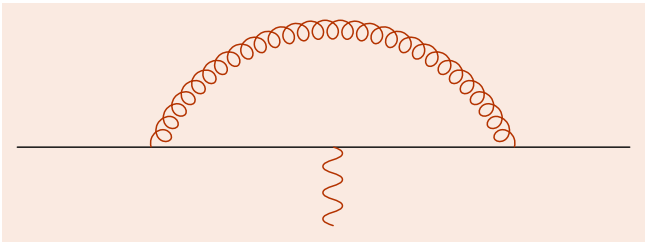

Fig. 28.2 G_0VG_0 contribution

Fig. 28.3 Green functions leading to derivative and perturbed orbital terms

energy shift, but there are two ways a residual double pole can be generated. The first comes from expanding

$$\Sigma(E) = \Sigma(\varepsilon_v) + (E-\varepsilon_v)\Sigma'(\varepsilon_v) + \ldots \quad (28.65)$$

and is called the derivative term. The second comes from restricting one of the "outside" propagators so that $m \neq v$, which again leads to a double pole. (The excluded term is associated with a cross term in the Taylor expansion of $1/(E-\Sigma_{vv}-E_Z)$.) This is referred to as a perturbed orbital term, since one can form a state $|\tilde{v}\rangle$ and show that the term is $\Sigma_{v\tilde{v}}(\varepsilon_v)+\Sigma_{\tilde{v}v}(\varepsilon_v)$. If written as

$$\Delta E_{PO} = \sum_{m\neq v}\left[\frac{\langle v|\Sigma|m\rangle\langle m|V|v\rangle}{\varepsilon_m-\varepsilon_v} + \frac{\langle v|V|m\rangle\langle m|\Sigma|v\rangle}{\varepsilon_m-\varepsilon_v}\right], \quad (28.66)$$

the close relation of the term to second-order Rayleigh–Schrödinger perturbation theory is seen.

The self-energy term discussed above has both the electron and the photon propagate from the same initial point to the same final point. Another term in which the photon propagates from x_1 to x_2, but the electron propagates from x_2 to the same point is present, called the vacuum polarization term. The diagram representing it is shown in Fig. 28.4. If one expands the electron propagator using Eq. (28.37), only terms with odd powers of V contribute. The term linear in V gives the bulk of the effect and is called the Uehling term. The exact calculation was considered in [33], where it was shown that a partial wave expansion can be formed of the difference of the full VP with the Uehling term. The resulting Wichmann–Kroll terms are quite small. The fact that the basic expression for vacuum polarization involves $G(E,\boldsymbol{x}_2,\boldsymbol{x}_2)$, which is very singular, was analyzed in [34]

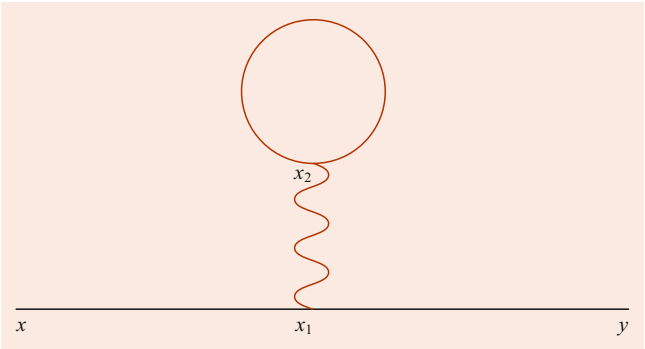

Fig. 28.4 Green function for vacuum polarization

using an alternative to dimensional regularization, Pauli–Villars regularization [35]. We present some details of the calculation, which illustrates charge renormalization.

Following the same steps as with the self-energy, we note that the energy of the photon line, cq_0, is now forced to vanish, which allows the $\boldsymbol{q}$ integration to be carried out, leading to a double pole with factor

$$E_{VP}^{(2)} = \mathrm{i}\alpha\hbar c \int \mathrm{d}\boldsymbol{x}_1 \mathrm{d}\boldsymbol{x}_2 \frac{\bar{\psi}_v(\boldsymbol{x}_1)\gamma_0\gamma_\mu\psi_v(\boldsymbol{x}_1)}{|\boldsymbol{x}_1 - \boldsymbol{x}_2|} \times \int \frac{\mathrm{d}z}{2\pi} \mathrm{Tr}[\gamma^\mu G(z, \boldsymbol{x}_2, \boldsymbol{x}_2)\gamma_0] \,. \tag{28.67}$$

The $\mu = 0$ component of this then describes the Coulomb field of the charge density of the state v interacting with an electron looping from the point of interaction back to the same point.

Pauli and *Villars* [35] analyzed the ultraviolet infinities of one-loop vacuum polarization and showed that they could be regularized by introducing two similar expressions, but with the electron mass ($m \equiv M_0$) replaced by either M_1 or M_2. If the two expressions are multiplied by the factors $(M_0^2 - M_2^2)/(M_2^2 - M_1^2)$ and $(M_1^2 - M_0^2)/(M_2^2 - M_1^2)$, respectively, and added to the original term, they showed the ultraviolet infinities were eliminated, and explicitly finite expressions could be analyzed. It is of interest to show how the calculation works for the case $M_1 = 20M_0$ and $M_2 = 30M_0$, even though they are understood to be taken to infinity after renormalization.

If one starts by considering the energy of a positive charge e in the Coulomb field of a fixed proton, one has $E_0(r) = \hbar c\alpha/r$. The effect of vacuum polarization on the energy breaks into two parts. One part is proportional to the lowest order energy,

$$E_1(r) = -\frac{2\alpha}{3\pi}\left[C_1 \ln\frac{M_1}{m} + C_2 \ln\frac{M_2}{m}\right]E_0(r) \equiv (Z_3 - 1)E_0(r) \,. \tag{28.68}$$

For the Pauli–Villars masses chosen, $Z_3 = 1.004\,138$. Even though in the limit of infinite masses this so-called photon renormalization constant is formally infinite, the smallness of α and the slow increase of the logarithm function make this formally infinite term close to 1 for the values chosen.

As with the electron mass renormalization, one must realize that this contribution is always present when two charges interact. If one could somehow suppress the effect of vacuum polarization, the effective elementary charge, which is called the bare charge e_0, would be smaller. The effect of $E_1(r)$ is to renormalize e_0 to the observed charge e through $e = e_0\sqrt{Z_3}$. Alternatively, one can simply work with the observed charge and drop E_1. In either case, the finite remainder is what of interest. The Uehling term is the term independent of C_1 and C_2 in

$$E_2(r) = -\frac{\alpha}{12\pi^2}E_0(r)\int_1^\infty \mathrm{d}t\sqrt{t^2-1}\left(\frac{1}{t^2} + \frac{2}{t^4}\right) \times \left[\mathrm{e}^{-2\frac{M_0c}{\hbar}tr} + C_1\mathrm{e}^{-2\frac{M_1c}{\hbar}tr} + C_2\mathrm{e}^{-2\frac{M_2c}{\hbar}tr}\right] . \tag{28.69}$$

It plays a role in the Lamb shift, and by itself would act to make the $2s$ state more strongly bound than the $2p_{1/2}$ state. The other two terms are small and can be shown to vanish quadratically for large values of the masses M_1, M_2.

Our using finite masses allows a central point about the renormalization program to be emphasized. As long as one works with renormalized quantities, finite calculations can be carried out. As shown in the example here, there is some dependence on the masses; however, there is little sensitivity to it, technically because of a quadratic falloff. A renormalizable theory in this picture should be thought of as insensitive to the high energy behavior: even if there is some new physics associated with the large momentum part of the loops, the predictions of a renormalizable theory like QED will change very little.

An important, relatively recent advance in exact calculations is in the two-loop Lamb shift. As with the one-loop case, both expansions in $Z\alpha$ and numerical treatments have been made. An example of a contribution is the overlapping loop diagram (Ov) shown in Fig. 28.5.

$$E_{SE}^{(4)}(\mathrm{Ov}) = \alpha^2c^4\int\frac{\mathrm{d}^4q_1}{(2\pi)^4}\frac{\mathrm{d}^4q_2}{(2\pi)^4}\frac{1}{q_1^2}\frac{1}{q_2^2}\int \mathrm{d}\boldsymbol{x}\,\mathrm{d}\boldsymbol{z}\,\mathrm{d}\boldsymbol{w} \times \mathrm{d}\boldsymbol{y}\,\bar{\psi}_v(\boldsymbol{x})\gamma_\mu G(\varepsilon_v - cq_{10}, \boldsymbol{x}, \boldsymbol{z}) \times \gamma^\nu G(\varepsilon_v - cq_{10} - cq_{20}, \boldsymbol{z}, \boldsymbol{w}) \times \gamma^\mu G(\varepsilon_v - q_{20}, \boldsymbol{w}, \boldsymbol{y})\gamma_\nu\psi_v(\boldsymbol{y})\mathrm{e}^{\mathrm{i}\boldsymbol{q}\cdot(\boldsymbol{x}-\boldsymbol{y})/\hbar} \,. \tag{28.70}$$

A striking feature of the expansion in $Z\alpha$ was the discovery of a very large coefficient by *Pachucki* [36], who found

$$E_{SE}^{(4)} = \frac{mc^2\alpha^2(Z\alpha)^4}{\pi^2n^3}[0.538\,941 - 21.554\,47(Z\alpha) + \ldots] \tag{28.71}$$

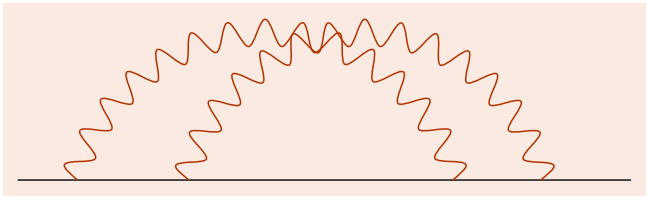

Fig. 28.5 Representative two-loop Lamb shift diagram

This emphasizes the need for the numerical approach for even moderate values of Z, as the above function changes sign by $Z = 4$. A recent discussion of the present status of two-loop calculations can be found in [37].

28.4 Two-Particle Bound States

We have so far dealt with hydrogen using the external field approximation, with the only role of the nucleus being the creation of a static Coulomb potential. We now will treat the nucleus dynamically, so that we must deal with two-particle bound states. To firstly justify the approximation, and secondly set up a perturbation theory to evaluate corrections to it, specifically recoil corrections, we now generalize $G_2(E, \boldsymbol{x}, \boldsymbol{y})$ from Eq. (28.41) to

$$\begin{aligned} &G_4(E, \boldsymbol{x}_1, \boldsymbol{x}_2, \boldsymbol{y}_1, \boldsymbol{y}_2) \\ &\quad = -\frac{\mathrm{i}}{\hbar} \int_{-\infty}^{\infty} \mathrm{d}t \mathrm{e}^{\mathrm{i}Et/\hbar} \langle 0|T(\psi_H(\boldsymbol{x}_1, t)\phi_H(\boldsymbol{x}_2, t) \\ &\qquad \times \bar{\psi}_H(\boldsymbol{y}_1, 0)\bar{\phi}_H(\boldsymbol{y}_2, 0))|0\rangle \ . \end{aligned} \tag{28.72}$$

Because the structure of the proton brings up issues not directly related to what we want to stress, it is convenient to treat it as a positive muon, so the field ϕ_H denotes that particle. No external field is now assumed, so the perturbation expansion will involve the free electron propagator, with mass denoted m_1, and the free muon propagator, with mass denoted m_2.

The argument given previously for $G_2(E, \boldsymbol{x}, \boldsymbol{y})$ showing that a pole is present carries through almost unchanged. The only difference is that to eliminate the time dependence from the product of the two operators one writes, after choosing $t > 0$ and inserting a complete set of states,

$$\begin{aligned} &\langle 0|\psi_H(\boldsymbol{x}_1, t)\phi_H(\boldsymbol{x}_2, t)|m\rangle \\ &\quad = \langle 0|\mathrm{e}^{\mathrm{i}Ht/\hbar}\mathrm{e}^{-\mathrm{i}Ht/\hbar}\psi_H(\boldsymbol{x}_1, t)\mathrm{e}^{\mathrm{i}Ht/\hbar}\mathrm{e}^{-\mathrm{i}Ht/\hbar} \\ &\qquad \times \phi_H(\boldsymbol{x}_2, t)\mathrm{e}^{\mathrm{i}Ht/\hbar}\mathrm{e}^{-\mathrm{i}Ht/\hbar}|m\rangle \\ &\quad = \langle 0|\psi_H(\boldsymbol{x}_1, 0)\phi_H(\boldsymbol{x}_2, 0)|m\rangle \mathrm{e}^{-\mathrm{i}E_m t/\hbar} \ . \end{aligned} \tag{28.73}$$

This argument can clearly be extended to a string of any number of operators, and the conclusion that a pole at $E = E_v$ is present is the same.

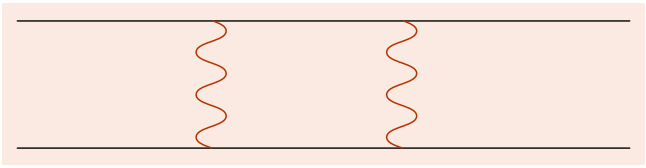

Fig. 28.6 Two-rung ladder diagram

We again begin by transforming to the interaction picture, but use Coulomb gauge rather than Feynman gauge. In lowest order,

$$\begin{aligned} &\langle 0|T(\psi(\boldsymbol{x}_1, t)\phi(\boldsymbol{x}_2, t)\bar{\psi}(\boldsymbol{y}_1, t')\bar{\phi}(\boldsymbol{y}_2, t'))|0\rangle \\ &\quad = -[S_F(\boldsymbol{x}_1, \boldsymbol{y}_1, t - t')]_1[S_F(\boldsymbol{x}_2, \boldsymbol{y}_2, t - t')]_2 \ , \end{aligned} \tag{28.74}$$

and we introduce a free propagator

$$\begin{aligned} &S_0(\boldsymbol{x}_1, \boldsymbol{x}_2, \boldsymbol{y}_1, \boldsymbol{y}_2, t - t')_{ab,cd} \\ &\quad = [S_F(\boldsymbol{x}_1, \boldsymbol{y}_1, t - t')]_{ab}[S_F(\boldsymbol{x}_2, \boldsymbol{y}_2, t - t')]_{cd} \ . \end{aligned} \tag{28.75}$$

Binding is associated with an infinite summation of Coulomb photon exchanges described by the function, now taking $t' = 0$,

$$\begin{aligned} &S_L(\boldsymbol{x}_1, \boldsymbol{x}_2, \boldsymbol{y}_1, \boldsymbol{y}_2, t)_{ab,cd} \\ &\quad = S_0(\boldsymbol{x}_1, \boldsymbol{x}_2, \boldsymbol{y}_1, \boldsymbol{y}_2, t)_{ab,cd} \\ &\qquad + \int \mathrm{d}\boldsymbol{w}_1 \mathrm{d}\boldsymbol{w}_2 \mathrm{d}t_w S_0(\boldsymbol{x}_1, \boldsymbol{x}_2, \boldsymbol{w}_1, \boldsymbol{w}_2, t - t_w)_{ae,cf} \\ &\qquad \cdot \gamma_{0eg}\gamma_{0fh}\frac{\alpha}{|\boldsymbol{w}_1 - \boldsymbol{w}_2|} S_L(\boldsymbol{w}_1, \boldsymbol{w}_2, \boldsymbol{y}_1, \boldsymbol{y}_2, t_w)_{gb,hd} \ . \end{aligned} \tag{28.76}$$

Expanding this leads to a set of terms whose Feynman diagrams look like a ladder, with the Coulomb interaction forming the rungs. A two-rung ladder is shown in Fig. 28.6.

Before analyzing S_L, it is useful to form the Green function of S_0 and analyze it. It is

$$\begin{aligned} &G_0(E, \boldsymbol{x}_1, \boldsymbol{x}_2, \boldsymbol{y}_1, \boldsymbol{y}_2) \\ &\quad = -\frac{\mathrm{i}}{\hbar} \int_{-\infty}^{\infty} \mathrm{d}t \mathrm{e}^{\mathrm{i}Et/\hbar} S_F^{(1)}(\boldsymbol{x}_1, t, \boldsymbol{y}_1, 0) S_F^{(2)}(\boldsymbol{x}_2, t, \boldsymbol{y}_2, 0) \\ &\quad = -\frac{\mathrm{i}}{\hbar} \int_{-\infty}^{\infty} \mathrm{d}t \int \frac{\mathrm{d}E_1}{2\pi} \int \frac{\mathrm{d}E_2}{2\pi} \mathrm{e}^{\mathrm{i}t(E - E_1 - E_2)/\hbar} \\ &\qquad \times [G_0(E_1, \boldsymbol{x}_1, \boldsymbol{y}_1)\gamma_0]_1[G_0(E_2, \boldsymbol{x}_2, \boldsymbol{y}_2)\gamma_0]_2 \\ &\quad = -\mathrm{i} \int \frac{\mathrm{d}E_1}{2\pi} [G_0(E_1, \boldsymbol{x}_1, \boldsymbol{y}_1)\gamma_0]_1 \\ &\qquad \times [G_0(E - E_1, \boldsymbol{x}_2, \boldsymbol{y}_2)\gamma_0]_2 \ . \end{aligned} \tag{28.77}$$

Using Eq. (28.35) and the decomposition given in Eq. (28.21) then gives

$$\begin{aligned} &G_0(E,\boldsymbol{x}_1,\boldsymbol{x}_2,\boldsymbol{y}_1,\boldsymbol{y}_2) \\ &\quad = -\mathrm{i}\frac{1}{\hbar^6}\int\frac{\mathrm{d}E_1}{2\pi}\int\frac{\mathrm{d}\boldsymbol{p}_1}{(2\pi)^3}\mathrm{e}^{\mathrm{i}\boldsymbol{p}_1\cdot(\boldsymbol{x}_1-\boldsymbol{y}_1)/\hbar}\int\frac{\mathrm{d}\boldsymbol{p}_2}{(2\pi)^3} \\ &\qquad \times \mathrm{e}^{\mathrm{i}\boldsymbol{p}_2\cdot(\boldsymbol{x}_2-\boldsymbol{y}_2)/\hbar}\left[\frac{\Lambda_+(\boldsymbol{p}_1)}{E_1-E_{p_1}+\mathrm{i}\delta}+\frac{\Lambda_-(\boldsymbol{p}_1)}{E_1+E_{p_1}-\mathrm{i}\delta}\right]_1 \\ &\qquad \times\left[\frac{\Lambda_+(\boldsymbol{p}_2)}{E-E_1-E_{p_2}+\mathrm{i}\delta}+\frac{\Lambda_-(\boldsymbol{p}_2)}{E-E_1+E_{p_2}-\mathrm{i}\delta}\right]_2 . \end{aligned} \tag{28.78}$$

Finally, using the Cauchy residue theorem to carry out the E_1 integration gives

$$\begin{aligned} &G_0(E,\boldsymbol{x}_1,\boldsymbol{x}_2,\boldsymbol{y}_1,\boldsymbol{y}_2) \\ &\quad = -\frac{1}{\hbar^6}\int\frac{\mathrm{d}\boldsymbol{p}_1}{(2\pi)^3}\mathrm{e}^{\mathrm{i}\boldsymbol{p}_1\cdot(\boldsymbol{x}_1-\boldsymbol{y}_1)/\hbar} \\ &\qquad \times\int\frac{\mathrm{d}\boldsymbol{p}_2}{(2\pi)^3}\mathrm{e}^{\mathrm{i}\boldsymbol{p}_2\cdot(\boldsymbol{x}_2-\boldsymbol{y}_2)/\hbar}\frac{[\Lambda_+(\boldsymbol{p}_1)]_1[\Lambda_+(\boldsymbol{p}_2)]_2}{E-E_{p_1}-E_{p_2}+\mathrm{i}\delta} \\ &\qquad -\frac{[\Lambda_-(\boldsymbol{p}_1)]_1[\Lambda_-(\boldsymbol{p}_2)]_2}{E+E_{p_1}+E_{p_2}-\mathrm{i}\delta} . \end{aligned} \tag{28.79}$$

The early calculations of recoil effects used this relatively complicated Green function. However, one has the freedom to work with simpler expressions, as long as the difference between the Green functions is accounted for in perturbation theory. The term with two factors of Λ_{--} is small and can be dropped. We further note that one can avoid the need to use the Cauchy residue theorem by the following manipulation. The Λ_{++} part of the muon propagator in Eq. (28.78) has a denominator that can be rewritten as

$$\begin{aligned} &\frac{1}{E-E_1-E_{p_2}+\mathrm{i}\delta} \\ &\quad = \left[\frac{1}{E-E_1-E_{p_2}+\mathrm{i}\delta}-\frac{1}{E-E_1-E_{p_2}-\mathrm{i}\delta}\right] \\ &\qquad +\frac{1}{E-E_1-E_{p_2}-\mathrm{i}\delta} \\ &\quad = -2\pi\mathrm{i}\delta(E_1-(E-E_{p_2}))+\frac{1}{E-E_1-E_{p_2}-\mathrm{i}\delta} . \end{aligned} \tag{28.80}$$

This motivates using an approximation to the muon propagator,

$$\begin{aligned} &[G_0(E-E_1,\boldsymbol{x}_2,\boldsymbol{y}_2)\gamma_0]_2 \\ &\quad \to -2\pi\mathrm{i}\delta(E_1-\tilde{E})\delta^3(\boldsymbol{x}_2-\boldsymbol{y}_2)\left[\frac{1+\gamma_0}{2}\right]_2 , \end{aligned} \tag{28.81}$$

where $\tilde{E}\equiv E-m_2c^2$. The term not involving the delta function has been dropped because it has a pole that is on the same side of the axis as the pole associated with the electron's positive projector term and, thus, fails to vanish only for the electrons negative energy projector, which gives a small result. For purposes of illustration, we have further approximated $E_{p_2}=m_2c^2$ and $\Lambda_{++}=\frac{1+\gamma_0}{2}$, the $m_2\to\infty$ limit, although for practical calculations, it is useful to retain some parts of the muon propagator. When this approximation is made in the ladder diagrams, the muon propagators essentially drop out of the calculation; the position variables are all forced to all be at the same place, which we choose as the origin. If one creates the Green function of S_L from Eq. (28.76), approximating the muon line as just described, it now effectively depends only on the electron variables, and one can show it satisfies

$$\begin{aligned} &G_L(E,\boldsymbol{x}_1,\boldsymbol{y}_1) \\ &\quad = G_0(E,\boldsymbol{x},\boldsymbol{y})\gamma_0 \\ &\qquad +\int\mathrm{d}\boldsymbol{w}G_0(E,\boldsymbol{x},\boldsymbol{w})\gamma_0\frac{\alpha\hbar c}{|\boldsymbol{w}|}G_L(E,\boldsymbol{w},\boldsymbol{y}) . \end{aligned} \tag{28.82}$$

The muon positive energy projector $[(1+\gamma_0)/2]_2$ is understood as a common factor. Outside of that factor, this equation is identical to that satisfied by the Coulomb Green function, leading to the expansion previous given in Eq. (28.37) when V is a Coulomb potential. However, we know that this Green function has poles at the Dirac eigenvalues, so although we started with free propagators, we now have an function of E that has poles at the nonrecoil values and can now start building in the effect of recoil.

Once we have a Green function that has bound state poles that approximate the full Green function, recoil corrections can be found in the way we described previously. Since now we can represent this approximated Green function as a spectral representation of the form in Eq. (28.31), although with the wave functions ψ_m we now have a muon component multiplied in, the goal (which involves some fairly complicated manipulations that we will not show here) is to set up an equation of the form

$$G_4 = G_L + G_L\delta K G_4 , \tag{28.83}$$

w here δK is formed from both pure "kernels", diagrams that cannot be split in two by a cut through the electron and muon lines (unlike Fig. 28.6) and the effect of simplifying the Green function. Approximating G_4 with G_L on the right-hand side can be seen to give a double pole, with an energy shift equal to the matrix element of δK.

An example of this kind of calculation applied to positronium hyperfine splitting is given in [38, 39]. The heart of the calculation involves the treatment of kernels with three exchanged photons in Coulomb gauge. The calculation was originally done by *Pachucki* [40], and while quite different

in many details, requires the evaluation of the same set of diagrams.

An important generalization of the Bethe–Salpeter approach is having the two bound particles being electrons in helium and accounting for the nucleus by using the Furry picture. This program was carried out by *Araki* [41] and *Sucher* [42]. As with recoil calculations, the basic step is consideration of an infinite ladder of Coulomb exchanges. In place of free propagators between the rungs, one has Coulomb Green functions. By carrying out approximations valid in the nonrelativistic limit one can form a Green function with poles at the nonrelativistic energies known from solving Eq. (28.1) for two electrons. As stressed earlier, because these lowest order energies can be determined with an accuracy far exceeding the level at which QED corrections enter, the study of these corrections is quite advanced. However, the present state-of-the-art calculations are carried out in the framework of NRQED, and we defer the discussion of helium to the concluding remarks.

28.5 Many-Electron Bound States

The incorporation of QED effects in many-electron bound states is a problem of fundamental interest, although as emphasized earlier, it must be possible to solve the Schrödinger equation with high accuracy. As a matter of principle, though, we now wish to show that the use of Green functions allows a QED approach to the many-electron problem. It now has to describe both radiative corrections and the exchange of photons between different electrons consistently.

An active subfield of QED is the study of highly charged ions, generally with two or more electrons remaining after the others have been stripped from a high Z atom. Relativistic and QED effects are enhanced in these ions, and a QED treatment is needed. In highly charged ions, the dominant effect on electrons is their attraction to the nucleus, and it can be shown that electron–electron interactions have a factor $1/Z$ and can be treated in perturbation theory. This can lead to situations where one can, indeed, study the larger QED effects relatively free of structure uncertainty, and the study of the spectra of some of these ions now provides tests of QED in intense Coulomb fields.

A treatment of the QED alternative to the Green function approach described here is afforded through S-matrix techniques [43, 44]. In these calculations, an adiabatic factor ε plays a central role. It is used to "turn off" H_I at large positive and negative times. An example of how it works for the sodium isoelectronic sequence is given in [45]. Here, we show some of the features of the Green function approach. To be specific we work with lithium-like ions and consider a six-point Green function. One starts with

$$G_6(E,\boldsymbol{x}_1,\boldsymbol{x}_2,\boldsymbol{x}_3,\boldsymbol{y}_1,\boldsymbol{y}_2,\boldsymbol{y}_3) = -\frac{\mathrm{i}}{\hbar}\int_{-\infty}^{\infty} \mathrm{d}t\,\mathrm{e}^{\mathrm{i}Et/\hbar}\langle 0|T(\psi_H(\boldsymbol{x}_1,t)\psi_H(\boldsymbol{x}_2,t)\psi_H(\boldsymbol{x}_3,t) \times \bar{\psi}_H(\boldsymbol{y}_1,0)\bar{\psi}_H(\boldsymbol{y}_2,0)\bar{\psi}_H(\boldsymbol{y}_3,0)))|0\rangle \ . \tag{28.84}$$

The formal treatment showing the presence of poles at $E = E_v$ is identical to the earlier discussion. To carry out calculations one uses the Furry or extended Furry picture, with either a Coulomb potential or some screened potential defining the states.

With many electrons present, these states are Slater determinants of occupied orbitals, and the starting point of QED calculations is the same as for MBPT calculations. The nonradiative QED terms, in fact, have a close relation to the MBPT expansion. For the example here, if considering the ground and first excited states, one would use

$$|V\rangle = b^\dagger{}_v b^\dagger{}_a b^\dagger{}_b|0\rangle \ , \tag{28.85}$$

with v being a $2s$, $2p_{1/2}$, or $2p_{3/2}$ state, and a and b the two spin states of the $1s$ state.

In lowest order, the energy should be the sum of the three energies of the populated states, in this case $\varepsilon_v + 2\varepsilon_a$. It actually takes a little work to show that the energies add, but the calculation is instructive. The lowest order Green function has three electron propagators, with associated integrals over E_1, E_2, and E_3. The t integration then gives a delta function of $E - E_1 - E_2 - E_3$. Using it to eliminate E_3, say, leaves an integral over E_1 and E_2 of the form

$$\int \frac{\mathrm{d}E_1}{2\pi}\int \frac{\mathrm{d}E_2}{2\pi}\frac{1}{E_1-\varepsilon_a+\mathrm{i}\delta}\frac{1}{E_2-\varepsilon_b+\mathrm{i}\varepsilon} \times \frac{1}{E-E_1-E_2-\varepsilon_v+\mathrm{i}\delta} \ . \tag{28.86}$$

Because the three states all have positive energy, the E_1 and E_2 integrations can be carried out with Cauchy's residue theorem, giving the expected factor

$$\frac{1}{E-E_v-E_a-E_b} \ . \tag{28.87}$$

One can then proceed finding double poles to find the shift of the energy.

The self-energy and vacuum polarization terms enter in the same way as for hydrogen, with the other electrons as "spectators". If the extended Furry picture is used, the Coulomb Green function cannot be used, and the Green function must be formed numerically. Unless the ion studied is

hydrogenic, one must account for the interaction between electrons. A perturbative treatment works well for highly charged ions that have a simple electronic structure, particularly ions with one valence electron and a filled core. In place of the helium treatment, where the Coulomb interaction between the electrons was treated to all orders, one calculates order by order, with diagrams roughly ordered by the number of photons present.

An example of how QED has been tested is provided by lithium-like bismuth. This is a case where QED calculations have been carried out [46, 47], and at the level of the one-loop Lamb shift, one can see that extra physics must be included. The accurate measurement required for QED effects to be studied was provided by measurements in the LLNL EBIT [48], where

$$E = 2788.139(39)\,\mathrm{eV} \tag{28.88}$$

was found for the $2p_{3/2} - 2s$ splitting.

Before including the Lamb shift, calculations not including it were carried out in a range of screening potentials. Despite starting off differently, inclusion of up to three-photon exchange diagrams led to a common answer of 2814.348 eV. As was mentioned above, the field theory treatment of photon exchange has an interesting relationship to MBPT. One photon exchange can be done in either Coulomb or Feynman gauge, with the latter being more convenient computationally. However, in Coulomb gauge, one can see that exchange of a Coulomb photon is exactly equivalent to first-order MBPT. Exchange of a transverse photon is again equivalent to the MBPT treatment of the Breit interaction, with retardation included. However, when two photons are exchanged between two electrons, one encounters diagrams of the form of Fig. 28.6, with the understanding that spectator electrons are present. When both photons are Coulomb photons, the same contour integral encountered in the recoil discussion arises. It is well defined, with the two positive energy projectors giving a standard second-order MBPT term, and the other part giving a small contribution. We stress this point because this is a case where the use of field theory automatically avoids a term that would arise if one included negative energy states in MBPT perturbation theory in a straightforward manner. In sums over states m and n, MBPT would appear to include terms with m positive and n negative energy, and those terms can have vanishing denominators. They do not occur in the field theory calculation because they have poles on the same side of the axis, and the contour integration can be chosen to avoid them, giving zero. The more complicated case of having two transverse photons is also of interest, having a history dating back to Breit's calculations of helium fine structure. The equation he used, named after him, suffers from problems similar to those just discussed, in particular leading to a term apparently of the order of the fine structure that had to be artificially removed. The integration is more complicated in this case, but the end result is that the two transverse photon term that appeared to be of the order of fine structure is reduced by a factor of α. This aspect of QED in atomic physics is just as important as the Lamb shift, although it does not require renormalization.

Because of the high charge of this ion, radiative corrections are now a one percent effect. They are dominated by the one-loop Lamb shift, which has to be treated with the numerical methods described earlier. However, while it is of the correct size, different potentials give differing answers. This disparity is removed to a large extent by including a set of "screening" diagrams, similar to Figs. 28.2 and 28.3, but with the lower photon line connecting to another electron. After including these (along with the effect of the counterterm Eq. (28.39) on the self-energy if extended Furry picture is used), a unique answer of −26.308 eV is found, taking theory to 2788.040 eV. This differs only slightly from experiment and shows that QED works even in very intense Coulomb fields. However, the experiment has sufficient accuracy to show clearly that extra physics must be accounted for.

Two obvious sources of known physics can account for the remaining discrepancy, recoil corrections and the two-loop Lamb shift. Remarkably, even though the bismuth nucleus is quite heavy, sophisticated recoil corrections are needed before the actual two-loop Lamb shift can be treated. These will be described in Sect. 28.6. After their removal an effect expected to be dominated by the $2s$ two-loop Lamb shift remains. As with the one-loop Lamb shift, an expansion in $Z\alpha$ could not be expected to be reliable, and exact numerical calculations had to be carried out. The result is consistent with experiment. The present status of that large-scale effort is described in [37].

28.6 Recoil Corrections at High Z

The first recoil calculations were carried out in the context of the Bethe–Salpeter equation. They relied heavily on expanding in powers of $Z\alpha$. For highly charged ions, $Z\alpha$ is no longer a small parameter, so the calculation of recoil corrections in hydrogenic ions with high Z requires the consideration of an infinite set of kernels rather than just a few. The problem was treated by *Grotch* and *Pachucki* in [49], and Bethe–Salpeter type calculations were done in [50] and [51]. The combinatoric problems are considerable, but the simplicity of the final expressions that result suggests that a simpler approach is possible. Such an approach was, indeed, found by *Shabaev* [52], and we describe it here.

The simplest way to derive the leading effect of the finite mass of the nucleus can be found in the context of classi-

cal mechanics, where in a system with N_e light particles of mass m (the electrons) and a heavy particle of mass M (the nucleus), one considers the heavy particle's nonrelativistic kinetic energy,

$$T_N = \frac{\vec{P}_N^2}{2M} , \tag{28.89}$$

and evaluates it in the center of mass system. In that frame, one can eliminate T_N through

$$\vec{P}_N \to -\sum_{i=1}^{N_e} \vec{p}_i \ . \tag{28.90}$$

Adding this to the nonrelativistic kinetic energy of the electrons (the first term in Eq. (28.1)) gives a total kinetic energy

$$T_{\rm tot} = \sum_{i=1}^{N_e} \frac{\vec{p}_i{}^2}{2m_r} + H_{\rm MP} , \tag{28.91}$$

where $m_r = m/(1 + m/M)$ is the reduced mass, and

$$H_{\rm MP} = \sum_{i \neq j} \frac{\vec{p}_i \cdot \vec{p}_j}{2M} \tag{28.92}$$

is the mass polarization Hamiltonian. When this classical argument is extended to nonrelativistic quantum mechanics, it incorporates recoil exactly. However, if one works in the approximation of keeping only m/M corrections, extending the classical argument described above to field theory allows recoil to be treated relativistically for both one and many-electron systems.

To generalize Eq. (28.90) to field theory, we first note that the electron momentum is now described as a single field operator,

$$\vec{p}_e = -{\rm i}\hbar \int {\rm d}^3x \, \psi^\dagger(x) \vec{\nabla} \psi(x) \ . \tag{28.93}$$

We also must include the electromagnetic field with the nuclear momentum in the usual way, with Eq. (28.89) now becoming

$$T_N \to \frac{|\vec{P}_N + Ze\vec{A}(\vec{0},t)|^2}{2M} \ . \tag{28.94}$$

The position of the nucleus is close to the origin, so $\vec{A}$ is evaluated there. Now the operation of going to the center of mass frame replaces $\boldsymbol{P}_N$ with the negative of Eq. (28.93),

$$\vec{P}_N \to -\vec{p}_e \ , \tag{28.95}$$

and we see that including the kinetic energy of the nucleus leads to three new interaction Hamiltonians, operators to be added to $\tilde{H}_I$,

$$H_R = H_R(CC) + H_R(CT) + H_R(TT) \ , \tag{28.96}$$

with

$$H_R(CC) = -\frac{\hbar^2}{2M} \int {\rm d}^3x \int {\rm d}^3y \, \psi^\dagger(\vec{x},t) \times \vec{\nabla}_x \psi(\vec{x},t) \cdot \psi^\dagger(\vec{y},t) \vec{\nabla}_y \psi(\vec{y},t) \ , \tag{28.97}$$

$$H_R(CT) = \frac{{\rm i}Ze\hbar}{M} \vec{A}(\vec{0},t) \cdot \int {\rm d}^3x \, \psi^\dagger(\vec{x},t) \vec{\nabla}_x \psi(\vec{x},t) \ , \tag{28.98}$$

and

$$H_R(TT) = \frac{Z^2e^2}{2M} \vec{A}(\vec{0},t) \cdot \vec{A}(\vec{0},t) \ . \tag{28.99}$$

We note the similarity of $H_R(CC)$ with the Coulomb part of the QED Hamiltonian H_C, Eq. (28.12).

Treating the new interaction Hamiltonians then to first order will account for all m/M corrections to all order in $Z\alpha$. One can equally well extend the calculations to many-electron ions, although accounting for the electron–electron interaction requires including as many factors coming from the initial interaction Hamilton as are required for convergence.

28.7 Concluding Remarks

Precision QED is presently a quite active field, and we have touched on only a few topics. Conferences on the subject are frequent, with the biannual International Conference on Precision Atomic Physics being of note; the interested reader should be able to access the talks given at them through the internet. A particularly active field involves applications of NRQED, which has been developed to quite a high level by a number of researchers. In these recent works, dimensional regularization is used in conjunction with the Foldy–Wouthuysen transformation along with powerful numerical methods that allow treatment of Green functions involving more than one electron. Of particular note is the completion of the treatment of helium fine structure in [53] to order $mc^2\alpha^7$, which can be used to determine the fine structure constant. More recently, we note the very large-scale calculation of the properties of singlet helium in [54]. What we wish to emphasize in closing is that the basic framework of QED as the theory underpinning our understanding of all electromagnetically bound states is in some sense simple, despite the extreme complexity of present calculations. We have discussed the two basic propagators, that of the electron and the photon, and the interaction Hamiltonian $H_I(t)$ given

in Eq. (28.24), and an approach based on a Feynman diagram treatment of Green functions to calculate the energies of bound states. That is all that is needed to describe a vast array of systems, and when they are simple enough, agreement with experiment at the ppm level is routinely found from just a few basic assumptions.

Acknowledgements Donald Yennie was working on the basic idea of using the Green function approach of the Bethe–Salpeter equation for atoms with many electrons, in particular using a two-time formalism. His unpublished paper "Bethe–Salpeter Approach to Atomic Physics", along with [19], shaped the treatment of QED given in this chapter.

References

1. Schwinger, J.: Selected Papers on Quantum Electrodynamics. Dover, New York (1958)
2. Schweber, S.: A very thorough treatment of the breakthrough is given in *QED and the Men who Made it*. Academic Press, London (2000)
3. Schwinger, J.: Phys. Rev. **73**, 416 (1948)
4. Brown, L.S., Gabrielse, G.: Rev. Mod. Phys. **58**, 233 (1986)
5. Aaij, R., et al.: LHCb collaboration. JHEP **11**, 90 (2015)
6. Anotognini, A., et al.: Science **339**(6118), 417 (2013)
7. Lindgren, I., Holmberg, J., Salomonson, S.: Theor. Chem. Acc. **134**, 123 (2015)
8. Eides, M.I., Grotch, H., Shelyto, V.A.: Theory of Light Hydrogic Bound States. Springer Tracts in Mod. Phys., vol. 222. Springer, Berlin, Heidelberg, New York (2007)
9. Eides, M.I., Grotch, H., Shelyto, V.A.: Theory of Light Hydrogic Bound States. Phys. Rep. **342**(2-3), 63 (2001)
10. Furry, W.: Phys. Rev. **81**, 115 (1951)
11. Jauch, J.M., Rohrlich, F.: See the discussion in Chapters 14 and 15 of *The Theory of Photons and Electrons*. Addison-Wesley, Cambridge (1955)
12. Salpeter, E.E.: Phys. Rev. **87**, 150 (1952)
13. Salpeter, E.E., Newcomb, W.A.: Phys. Rev. **87**, 150 (1952)
14. Salpeter, E.E., Bethe, H.A.: Phys. Rev. **84**, 1232 (1951)
15. Caswell, W., Lepage, G.P.: Phys. Lett. B. **167**, 437 (1986)
16. Blundell, S.A., Guo, D.S., Johnson, W.R., Sapirstein, J.: Data Tables. At. Data Nucl. **37**, 103 (1987)
17. Kelly, H.P.: Phys. Rev. **131**, 684 (1963)
18. Shabaev, V.M.: Phys. Rep. **356**, 119 (2002)
19. Yennie, D.R.: AIP Conference Proceedings No. 189. American Institute of Physics, New York (1989). p. 393, and unpublished
20. Lamb, W.E., Retherford, R.C.: Phys. Rev. **72**, 241 (1947)
21. t'Hooft, G., Veltman, M.: Nucl. Phys. B. **44**, 189 (1972)
22. Drake, G.W.F., Swainson, R.A.: Phys. Rev. A **41**, 1243 (1990)
23. Brown, G.E., Mayers, D.F.: Proc. R. Soc. Lond. Ser. A **251**, 92 (1951)
24. Desiderio, A.M., Johnson, W.R.: Phys. Rev. A **14**, 1943 (1976)
25. Jentschura, U.D., Mohr, P.J., Soff, G.: Phys. Rev. A **63**, 042512 (2001)
26. Yerokhin, V.A., Shabaev, V.M.: J. Phys. Chem. Ref. Data **44**, 0033103 (2015)
27. Yerokhin, V.A., Pachucki, K., Shabaev, V.M.: Phys. Rev. A **72**, 042502 (2005)
28. Blundell, S.A., Snyderman, N.: Phys. Rev. A **44**, R1427 (1991)
29. Mohr, P.J.: Ann. Phys. (ny) **88**, 26 (1974)
30. Blundell, S.A., Cheng, K.T., Sapirstein, J.: Phys. Rev. A **55**, 1857 (1997)
31. Indelicato, P., Mohr, P.J.: Phys. Rev. A **63**, 052507 (2001)
32. Indelicato, P., Mohr, P.J.: Phys. Rev. A **58**, 165 (1998)
33. Wichmann, E.H., Kroll, N.M.: Phys. Rev. **101**, 843 (1956)
34. Indelicato, P., Mohr, P., Sapirstein, J.: Phys. Rev. A **89**, 042021 (2014)
35. Pauli, W., Villars: Rev. Mod. Phys. **21**, 434 (1949)
36. Pachucki, K.: Phys. Rev. Lett. **72**, 3154 (1994)
37. Yerokhin, V.A.: Phys. Rev. A **97**, 052509 (2018)
38. Adkins, G.A., Sapirstein, J.: Phys. Rev. A **58**, 3552 (1998)
39. Adkins, G.A., Sapirstein, J.: Phys. Rev. A **61**, 069902 (2000). (E)
40. Pachucki, K.: Phys. Rev. A **56**, 297 (1997)
41. Araki, H.: Prog. Theor. Phys. **17**, 619 (1957)
42. Sucher, J.: PhD thesis. Columbia University, New York City (1957)
43. Gell-Mann, M., Low, F.: Phys. Rev. **84**, 350 (1951)
44. Sucher, J.: Phys. Rev. **107**, 1448 (1957)
45. Sapirstein, J., Cheng, K.T.: Phys. Rev. A **91**, 062508 (2015)
46. Sapirstein, J., Cheng, K.T.: Phys. Rev. A **64**, 022502 (2001)
47. Yerokhin, V.A., Artemyev, A.N., Beier, T., Plunien, G., Shabaev, V.M., Soff, G.: Phys. Rev. A **60**, 3522 (1999)
48. Beiersdorfer, P., Osterheld, A.L., Scofield, J.H., Crespo Lopez-Urrutia, J.R., Widmann, K.: Phys. Rev. Lett. **80**, 3022 (1998)
49. Pachucki, K., Grotch, H.: Phys. Rev. **51**, 1854 (1995)
50. Shabaev, V.M., Artemyev Beier Soff, A.N.T.G.: J. Phys. B **31**(8), L337 (1998)
51. Adkins, G.S., Morrison, S., Sapirstein, J.: Phys. Rev. A **76**, 042508 (2007)
52. Shabaev, V.M.: Phys. Rev. A **57**, 59 (1998)
53. Pachucki, K., Yerokhin, V.A.: Phys. Rev. Lett. **104**, 070403 (2010)
54. Pachucki, K., Patkos, V., Yerokhin, V.A.: Phys. Rev. A **95**, 012508 (2017)

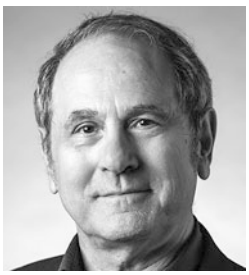

Jonathan R. Sapirstein Dr Sapirstein earned his PhD from Stanford University in 1979. He did postdoctoral work at UCLA and Cornell and has been at the University of Notre Dame, Indiana, since 1984. His current research interests are parity nonconservation in atoms, QED effects in highly charged many-electron ions, and QED calculations in hydrogen, positronium, muonium, and helium. Dr Sapirstein is a Fellow of the American Physical Society.